Detecting UWB Signals Using Cyclic Features

Yiyin Wang*†, Xiaoli Ma*, and Qi Zhou*

*School of Electrical and Computer Engineering, Georgia Institute of Technology
Atlanta, GA 30332-0250, USA
†Department of Automation, Shanghai Jiao Tong University, Shanghai, 200240, P. R. China

***Abstract*—Ultra wideband (UWB) signals facilitate efficient spectrum usage via coexistence with other narrowband signals. The detection of UWB signals under the coexistent narrowband signals is extremely important for UWB commercial and military purposes. Inherent cyclostationarity of the UWB signals provides unique features different from those of narrowband signals. In this paper, we investigate the cyclic features of a generalized UWB impulse radio (IR) signal. In order to detect UWB IRs under the existence of a narrowband signal (e.g. a GMSK signal), we explore both the nonconjugate and the conjugate cyclostationarity. A multi-cycle detector is proposed in time-domain making use of the conjugate cyclic autocorrelation to detect the UWB signal under the existence of the GMSK signal. The simulation results indicate the possibility to detect the UWB signal which is overwhelmed by the GMSK signal.**

I. Introduction

Ultra wideband (UWB) technology enables short-range high-rate communications and accurate localization. It is featured with extremely low transmission power and low probability of detection. The coexistence of UWB and narrowband signals is of great importance to make an efficient use of rare spectrum [1]–[3]. The detection and avoidance (DAA) scheme [2] is proposed for UWB devices to detect the presence of primary users (in general narrowband signals), and avoid the occupied spectrum. In contrast, to detect a UWB signal under the existence of narrowband signals is equally important for UWB commercial and military purposes. It is not a trivial task due to the distinctive properties of the UWB signals, and yet to be well explored.

As cyclostationarity exists in almost all modulated signals, it is widely used to detect various types of signals [4]–[6]. Moreover, the detectors based on cyclic features are robust to noise uncertainties. Recently, cyclostationary spectrum sensing becomes popular for cognitive radios (CRs) to detect the signals of interest. Detectors based on the cyclostationarity of orthogonal frequency division multiplexing (OFDM) signals are proposed in [3], [7], [8]. Gaussian minimum-shift keying (GMSK) modulated GSM systems are distinguished from the OFDM-based WLAN by their cyclic features [9]. Furthermore, compressive sampling is applied to recover the cyclic spectrum of wideband signals, and a cyclic feature detector is developed correspondingly to accomplish signal detection [10].

In this paper, we first investigate the cyclic features of a generalized UWB impulse radio (IR) signal, and achieve a closed-form expression of its spectrum-correlation density (SCD) starting from its covariance function. A few examples of the cyclic spectrum of the binary pulse-position modulation (BPPM) UWB IRs are shown and compared to the cyclic spectrum calculated based on the autocorrelation function [11]. In order to detect the UWB signal under the existence of a narrowband signal (e.g. GMSK signals), we explore both the nonconjugate and the conjugate cyclostationarity of the signals. Since the conjugate cyclostationarity of the GMSK signal is very faint compared to that of the UWB signal, we propose a multi-cycle detector in time-domain making use of the conjugate cyclic autocorrelation. The simulation results indicate that even when the power of the UWB signal is very small relative to the power of the GMSK signal, it is still possible to detect the UWB signal by exploiting the conjugate cyclostationarity.

II. System Model

An equivalent baseband model of a generalized UWB signal using pulse-amplitude modulation (PAM) or/and pulse-position modulation (PPM) can be written as

$$x(t) = \sum_{n=-\infty}^{+\infty} a_n g(t - nT_s - b_n\Delta - \epsilon), \tag{1}$$

where ϵ is the unknown deterministic timing offset. The symbol sequences a_n and b_n modulate the pulse amplitude and the pulse position, respectively. They are further assumed to be wide-sense stationary (WSS) and independent from each other. Moreover, the time interval Δ is the position shift for the PPM, and $g(t)$ is the symbol waveform of length T_s. Each symbol is composed of N_f frames. Each frame of length T_f accommodates a UWB pulse, and thus $T_s = N_f T_f$. The frame is further divided into N_c chips. The chip duration is T_c, where $T_c > T_p$ and $T_f = N_c T_c$. Without loss of generality, a symbol waveform employing both the direct sequence (DS) and time-hopping (TH) codes is given by

$$g(t) = \sum_{i=0}^{N_f-1} c_i p(t - iT_f - d_i T_c), \tag{2}$$

where $p(t)$ is the UWB pulse of width T_p, $c_i \in \{\pm 1\}$ is the DS code and $d_i \in [0, N_c - 1]$ is the TH code. Each user is uniquely assigned a DS and a TH code. If only the DS or the TH code is employed, then $d_i = 0, \forall i$ or $c_i = 1, \forall i$. Thus, the

codes are repeatedly used for each symbol. Note that $g(t)$ is a deterministic waveform for each user.

As a result, $x(t)$ can be viewed as the output of a signal $s(t)$ filtered by a pulse shaper, whose impulse response is $g(t)$. The signal $s(t)$ is given by

$$s(t) = \sum_{n=-\infty}^{+\infty} a_n \delta(t - nT_s - b_n\Delta - \epsilon), \tag{3}$$

where $\delta(t)$ is the delta function. Since a_n and b_n are WSS and independent from each other, it is well-known that $s(t)$ is cyclostationary with the fundamental cycle $1/T_s$. According to the input-output spectrum-correlation density (SCD) relation for filtering [4], we arrive at

$$S_x(\alpha, f) = G(f + \alpha/2)G^*(f - \alpha/2)S_s(\alpha, f), \tag{4}$$

where $G(f)$ is the Fourier transform of $g(t)$, and $S_x(\alpha, f)$ and $S_s(\alpha, f)$ are the cyclic spectrum of the signal $x(t)$ and $s(t)$, respectively.

III. Cyclic Spectrum Analysis

Now let us first investigate the cyclic spectrum of $s(t)$. The covariance function $C_s(t, \tau)$ of $s(t)$ is given by

$$\begin{aligned} & C_s(t, \tau) \\ = \; & E[s(t + \tau/2)s^*(t - \tau/2)] - \bar{s}(t + \tau/2)\bar{s}^*(t - \tau/2), \end{aligned} \tag{5}$$

where $\bar{s}(t) = E[s(t)]$. Thus, we define the autocorrelation function as $R_s(t, \tau) = E[s(t + \tau/2)s^*(t - \tau/2)]$ and $\bar{R}_s(t, \tau) = \bar{s}(t + \tau/2)\bar{s}^*(t - \tau/2)$. We remark that the covariance function $C_s(t, \tau)$ is employed to calculate the cyclic spectrum instead of the autocorrelation function $R_s(t, \tau)$ as in [11]. Since the PPM UWB signals with or without the TH codes may not be zero mean, the cyclic spectrum based on the covariance function may take the benefit of eliminating the cross terms of the noise and the signal mean. The estimate of the cyclic spectrum based on the covariance function may have a smaller error variance. Furthermore, the definition of $C_s(t, \tau)$ in (5) is called the nonconjugate covariance function. Correspondingly, the conjugate covariance function is given by

$$\begin{aligned} & C_s^*(t, \tau) \\ = \; & E[s(t + \tau/2)s(t - \tau/2)] - \bar{s}(t + \tau/2)\bar{s}(t - \tau/2). \end{aligned} \tag{6}$$

Therefore, the cyclic autocorrelation function (CAF) and the SCD based on (6) are named as the conjugate CAF and the conjugate SCD, which are denoted by the upper subscript $*$.

As the UWB signal is a real-value signal, the nonconjugate and conjugate SCD will be the same. Thus, we explore their nonconjugate cyclic features in the following. Based on (5), the cyclic spectrum of $s(t)$ can also be decomposed as

$$S_s(\alpha_q, f) = S_s^1(\alpha_q, f) - S_s^2(\alpha_q, f), \tag{7}$$

where $S_s^1(\alpha_q, f)$ and $S_s^2(\alpha_q, f)$ are the cyclic spectrum corresponding to $R_s(t, \tau)$ and $\bar{R}_s(t, \tau)$, respectively. Let us define $S_x^1(\alpha_q, f)$ and $S_x^2(\alpha_q, f)$ accordingly. To adopt the results in [11], we define parameters as follows. Recalling that a_n and b_n are assumed to be WSS and independent from each other, let us define $\bar{a} = E[a_n]$, $R_a(k) = E[a_n a_{n-k}^*]$, $\beta_n(f) = e^{-j2\pi\Delta f b_n}$, and $\bar{\beta}(f) = E[\beta_n(f)]$. The cyclic set is denoted as $\{\alpha_q, q = 0, \pm 1, \pm 2, \dots\}$, where $\alpha_q = q/T_s$. As a result, $S_x^1(\alpha_q, f)$ is given by [11]

$$\begin{aligned} & S_x^1(\alpha_q, f) \\ = \; & \frac{1}{T_s} e^{-j2\pi\alpha_q\epsilon} G(f + \frac{\alpha_q}{2}) G^*(f - \frac{\alpha_q}{2}) \Big\{ R_a(0)\bar{\beta}(\alpha_q) \\ & + \bar{\beta}(f + \frac{\alpha_q}{2})\bar{\beta}^*(f - \frac{\alpha_q}{2}) \big(S_a(T_s f - q/2) - R_a(0) \big), \end{aligned} \tag{8}$$

where $S_a(f) = \sum_{k=-\infty}^{+\infty} e^{-j2\pi k f} R_a(k)$ the power spectral density of a_n. Note that we do not decompose a_n as the sum of $\widetilde{a}_n$ and $\bar{a}$ in [11]. Hence, $S_x^1(\alpha_q, f)$ includes both the continuous and discrete spectrum components defined in [11].

To further investigate $\bar{R}_s(t, \tau)$ and its corresponding $S_s^2(\alpha_q, f)$, we make use of $\delta(t - a) = \int e^{j2\pi(t-a)f} df$. Denoting $m = n - k$, we derive $\bar{R}_s(t, \tau)$ as

$$\begin{aligned} & \bar{R}_s(t, \tau) \\ = \; & \sum_{n=-\infty}^{+\infty} \sum_{m=-\infty}^{+\infty} E[a_n \int e^{j2\pi(t+\tau/2-nT_s-b_n\Delta-\epsilon)y} dy] \\ & \times E[a_m^* \int e^{j2\pi(t-\tau/2-mT_s-b_m\Delta-\epsilon)z} dz] \\ = \; & \sum_{n=-\infty}^{+\infty} \sum_{m=-\infty}^{+\infty} \int\int e^{j2\pi(t(y+z)+\tau/2(y-z)-T_s(ny+mz)-\epsilon(y+z))} \\ & \times E[a_n e^{-j2\pi b_n \Delta y}] E[a_m^* e^{-j2\pi b_m \Delta z}] dy dz \\ = \; & \sum_{n=-\infty}^{+\infty} \sum_{k=-\infty}^{+\infty} \int\int e^{j2\pi(t(y+z)+(y-z)\tau/2-T_s(n(y+z)-kz)-\epsilon(y+z))} \\ & \times \bar{a}\bar{a}^* \bar{\beta}(y)\bar{\beta}(z) dy dz. \end{aligned} \tag{9}$$

According to the Poisson sum formula $\sum_{n=-\infty}^{+\infty} e^{-j2\pi n f T} = \frac{1}{T} \sum_{q=-\infty}^{+\infty} \delta(f - \frac{q}{T})$, $\bar{R}_s(t, \tau)$ can be simplified with respect to (w.r.t) n summation as

$$\begin{aligned} & \bar{R}_s(t, \tau) \\ = \; & \frac{1}{T_s} \sum_{k=-\infty}^{+\infty} \bar{a}\bar{a}^* \int\int e^{j2\pi(t(y+z)+(y-z)\tau/2+T_s kz-\epsilon(y+z))} \\ & \times \bar{\beta}(y)\bar{\beta}(z) \sum_{q=-\infty}^{+\infty} \delta(y + z - \frac{q}{T_s}) dy dz \\ = \; & \frac{1}{T_s} \sum_{q=-\infty}^{+\infty} \sum_{k=-\infty}^{+\infty} \int e^{j2\pi(t\frac{q}{T_s}+\tau(\frac{q}{2T_s}-z)+T_s kz-\epsilon\frac{q}{T_s})} \\ & \times \bar{a}\bar{a}^* \bar{\beta}(\frac{q}{T_s} - z)\bar{\beta}(z) dz. \end{aligned} \tag{10}$$

Furthermore, $\bar{s}(t) = E[s(t)]$ is periodic as well, since it can

be expanded by the Fourier series as

$$\begin{aligned}\bar{s}(t) &= \sum_{n=-\infty}^{+\infty} E[a_n \delta(t - nT_s - b_n\Delta - \epsilon)] \qquad (11)\\ &= \sum_{n=-\infty}^{+\infty} \bar{a} \int e^{j2\pi(t-nT_s-\epsilon)f} E[e^{-j2\pi b_n \Delta f}] df \\ &= \frac{1}{T_s}\bar{a} \sum_{q=-\infty}^{+\infty} \bar{\beta}(\frac{q}{T_s}) e^{j2\pi(t-\epsilon)\frac{q}{T_s}},\end{aligned}$$

where $\bar{a}\bar{\beta}(\alpha_q)$ is the Fourier coefficient for $\bar{s}(t)$ at the frequency α_q.

Consequently, the cyclic covariance function $\bar{R}_s(\alpha_q, \tau)$, which is the Fourier series of $\bar{R}_s(t, \tau)$ w.r.t t, can be derived as

$$\begin{aligned}&\bar{R}_s(\alpha_q, \tau) \qquad (12)\\ &= \frac{\bar{a}\bar{a}^*}{T_s} \sum_{k=-\infty}^{+\infty} \int e^{j2\pi(\tau(\frac{\alpha_q}{2}-z)+T_s k z - \epsilon\alpha_q)} \bar{\beta}(\alpha_q - z)\bar{\beta}(z) dz.\end{aligned}$$

Therefore, the cyclic spectrum $S_s^2(\alpha_q, f)$ corresponding to the Fourier transform of $\bar{R}_s(\alpha_q, \tau)$ w.r.t. τ, can be obtained as

$$\begin{aligned}&S_s^2(\alpha_q, f) \qquad (13)\\ &= \frac{\bar{a}\bar{a}^*}{T_s} \sum_{k=-\infty}^{+\infty} \\ &\quad \times \int \delta(f - \frac{\alpha_q}{2} + z) e^{j2\pi(T_s k z - \epsilon\alpha_q)} \bar{\beta}(\alpha_q - z)\bar{\beta}(z) dz \\ &= \frac{\bar{a}\bar{a}^*}{T_s} \bar{\beta}(f + \alpha_q)\bar{\beta}(\frac{\alpha_q}{2} - f) \sum_{k=-\infty}^{+\infty} e^{-j2\pi(T_s k(f - \frac{\alpha_q}{2}) + \epsilon\alpha_q)}.\end{aligned}$$

Making use of the Poisson sum formula again, we can further simplify $S_s^2(\alpha_q, f)$ as

$$\begin{aligned}S_s^2(\alpha_q, f) = &\frac{\bar{a}\bar{a}^*}{T_s^2} e^{-j2\pi\alpha_q\epsilon} \bar{\beta}(f + \frac{\alpha_q}{2})\bar{\beta}^*(f - \frac{\alpha_q}{2}) \qquad (14)\\ &\times \sum_{l=-\infty}^{+\infty} \delta(f - \frac{\alpha_q}{2} - \frac{l}{T_s}),\end{aligned}$$

$$S_s^2(\alpha_q, \frac{\alpha_q}{2} + \alpha_l) = \frac{\bar{a}\bar{a}^*}{T_s^2} e^{-j2\pi\alpha_q\epsilon} \bar{\beta}(\alpha_{q+l})\bar{\beta}^*(\alpha_l), \qquad (15)$$

where $S_s^2(\alpha_q, \frac{\alpha_q}{2} + \alpha_l)$ is composed of discrete spectrum lines. Note that $S_s^2(\alpha_q, \frac{\alpha_q}{2} + \alpha_l)$ equals to zero, when a_n is zero-mean WSS sequence.

Now we have all ingredients to achieve $S_x(\alpha_q, f)$ as

$$S_x(\alpha_q, f) = S_x^1(\alpha_q, f) - S_x^2(\alpha_q, f), \qquad (16)$$

where $S_x^1(\alpha_q, f)$ is given by (8) and

$$\begin{aligned}&S_x^2(\alpha_q, \frac{\alpha_q}{2} + \alpha_l) \qquad (17)\\ &= \frac{\bar{a}\bar{a}^*}{T_s^2} e^{-j2\pi\alpha_q\epsilon} G(\alpha_{q+l}) G^*(\alpha_l) \bar{\beta}(\alpha_{q+l})\bar{\beta}^*(\alpha_l).\end{aligned}$$

The cyclic spectrum of $S_x(\alpha_q, f)$ is decided by $G(f)$, $\bar{\beta}(f)$ and $S_a(f)$ together. Note that $G(f)$ plays an important role in the cyclic spectrum. Since $g(t)$ is a symbol waveform composed of UWB pulses, its bandwidth is decided by the UWB pulse. Furthermore, $\bar{x}(t) = E[x(t)]$ is periodic as well, thus it can be expanded by the Fourier series as

$$\bar{x}(t) = \frac{1}{T_s}\bar{a} \sum_{q=-\infty}^{+\infty} G\left(\frac{q}{T_s}\right) \bar{\beta}\left(\frac{q}{T_s}\right) e^{j2\pi(t-\epsilon)\frac{q}{T_s}}. \qquad (18)$$

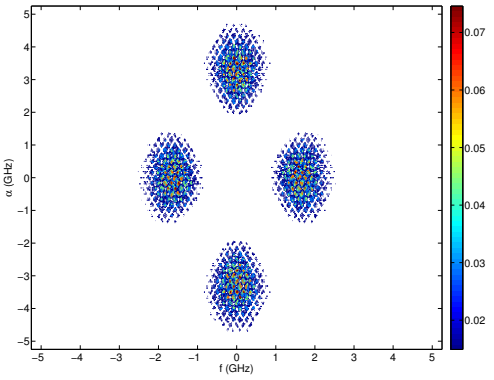

Fig. 1. The $S_x(\alpha, f)$ of a BPPM UWB signal with the TH and DS codes

Now let us show some examples of the cyclic spectrum. We further assume that a_n and b_n select values from the set $\{\pm 1\}$ and $\{0, 1\}$ with equal probability, respectively. Thus, the binary PAM (BPAM) and the BPPM are accommodated. For a_n sequence, $\bar{a} = 0$, $R_a(k) = \delta(k)$ and $S_a(f) = 1$. Moreover, $\bar{\beta}(f) = (1 + e^{-j2\pi f\Delta})/2$. Because $\bar{a}$ equals to zero, the discrete cyclic spectrum component $S_x^2(\alpha_q, \frac{\alpha_q}{2} + \alpha_l)$ vanishes for the BPAM or BPAM-BPPM UWB signal. In those cases, the SCD functions respectively based on the covariance and the autocorrelation function are the same. Thus, we show examples of the cyclic spectrum of the BPPM UWB signals using both the TH and DS codes with nonzero mean.

Examples 1: the second-derivative Gaussian pulse with the main lobe width of 0.6 ns is employed. Other parameters are assigned as $N_f = 8$, $N_c = 4$, $T_c = 2$ ns, $T_f = N_c T_c = 8$ ns, $T_s = N_f T_f = 64$ ns, and $\Delta = T_s/2 = 32$ ns. The sampling frequency is 10 GHz. We consider noiseless scenarios. Fig. 1 illustrates the cyclic spectrum of the BPPM UWB signals with TH and DS codes. When α_q equals to zero, the SCD is equivalent to the conventional spectrum density. Under such circumstances, the second-derivative Gaussian pulse, which is a bandpass signal, determines the location and the width of the occupied band. Consequently, the cyclic spectrum of the UWB signal spreads to a wide range in a diamond shape, which is composed of four components. Fig. 2 and 3 denote the details of $S_x(\alpha, f)$ and $S_x^1(\alpha, f)$, which are based on the covariance and autocorrelation functions respectively. We observe the spectrum components at multiple cycles of $1/T_s$. The cyclic feature is more clear for $S_x(\alpha, f)$ in Fig. 2. Higher peaks appear at $S_x^1(\alpha, f)$ in Fig. 3 as the contribution from the sequence mean $\bar{x}(t)$.

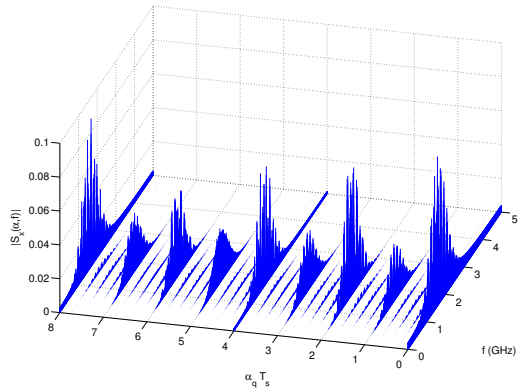

Fig. 2. The $S_x(\alpha, f)$ of a BPPM UWB signal with the TH and DS codes

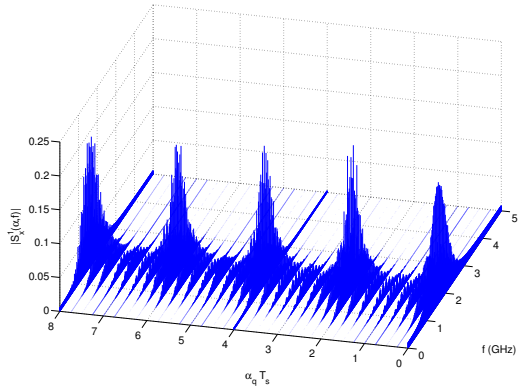

Fig. 3. The $S_x^1(\alpha, f)$ of a BPPM UWB signal with the TH and DS codes

IV. Detect UWB signal with the existence of GMSK signal

Our goal is to detect the UWB signal under the existence of a narrow band signal. Here, we consider a GMSK signal, which is widely adopted in GSM systems. An equivalent baseband model of the GMSK signal is [9]

$$u(t) = \exp\left\{ j2\pi h \sum_{n=-\infty}^{\infty} d_n \int_{-\infty}^{t} q(\tau - nT_g) d\tau \right\}, \quad (19)$$

where h is the modulation index and set to 0.5 as a two-level FSK, d_n is the information symbol belonging to $\{\pm 1\}$, the symbol period is T_g, and the pulse $q(t)$ is given by

$$q(t) = \frac{1}{T_g} \text{rect}(\frac{t}{T_g}) * p_G(t), \quad (20)$$

with $p_G(t)$ is the Gaussian pulse with the time bandwidth product BT (e.g. BT is assigned to 0.3). The Gaussian pulse $p_G(t)$ is cut to a length of $4T_g$. Therefore, the aggregate signal is the summation of the UWB signal and the GMSK signal as

$$z(t) = x(t) + u(t). \quad (21)$$

Note that the GMSK signal exhibits different nonconjugate and conjugate cyclostationarity as justified in [9]. On the other hand, the UWB signal maintains the same nonconjugate and conjugate cyclostationarity, since it is a real signal. Making use of this difference between them, we find out the GMSK signal dominates the nonconjugate cyclostationarity, and the UWB signal plays the key role in the conjugate cyclostationarity.

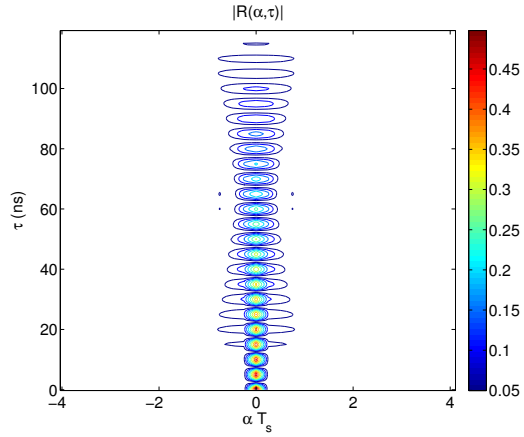

Fig. 4. The nonconjugate CAF $R(\alpha, \tau)$ of the BPAM UWB signal with the GMSK signal

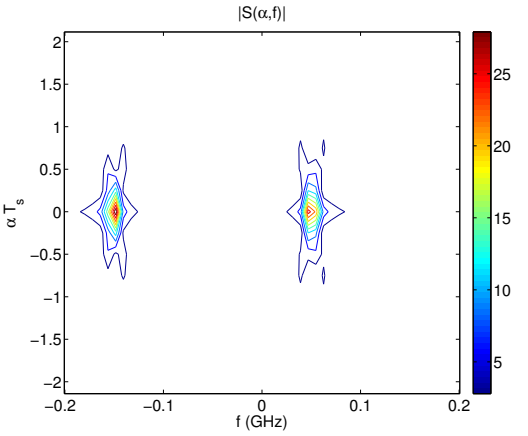

Fig. 5. The nonconjugate SCD $S(\alpha, f)$ of the BPAM UWB signal with the GMSK signal

Example 2: Figs. 4 and 5 show the contours of the nonconjugate cyclostationarity properties of $z(t)$, and Figs. 6 and 7 denote the conjugate case. The simulation parameters for these figures are as follows. For the UWB signal, an eighth-order Butterworth pulse with a 3 dB bandwidth of 500 MHz is employed. Thus, the sampling frequency is 2 GHz. No DS or TH code is used. Each symbol transmits a BPAM UWB pulse. The symbol period is 32 ns. Hence the basic cycle frequency is $1/T_s = 31.25$ MHz. The GMSK signal is of a bandwidth 200 KHz and a symbol rate 270.833 KHz. It is shifted by a carrier frequency of 50 MHz. Therefore, it is just in the band of interest of the UWB signal. The total length of the signal is $100\,\mu$s. The signal-to-interference ratio (SIR) is defined as the power of the UWB signal to the power of the GMSK signal. In these figures, SIR $= -10$ dB.

In order to estimate the cyclostationary properties, the signal is cut into L segments, where each segment contains four

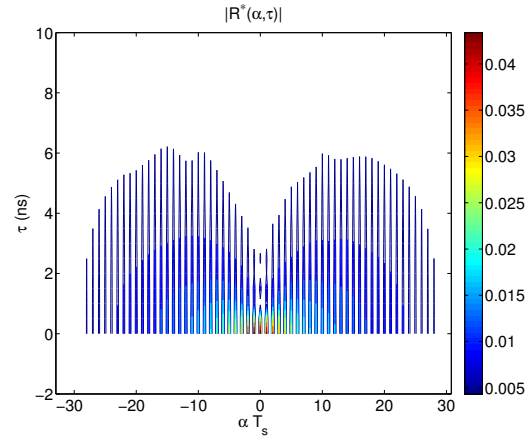

Fig. 6. The conjugate CAF $R^*(\alpha, f)$ of the BPAM UWB signal with the GMSK signal

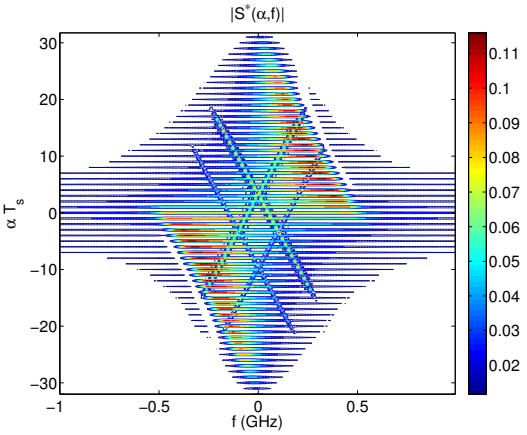

Fig. 7. The conjugate SCD $S^*(\alpha, f)$ of the BPAM UWB signal with the GMSK signal

UWB symbols (256 samples) and N denotes the number of samples per segment ($N = 256$). As a result, the nonconjugate covariance function can be estimated as

$$\hat{\mathbf{C}} = \frac{1}{L}\sum_{l=0}^{L-1}\mathbf{z}(l)\mathbf{z}^H(l) - \bar{\mathbf{z}}\bar{\mathbf{z}}^H, \tag{22}$$

where $\bar{\mathbf{z}} = (1/L)\sum_{l=0}^{L-1}\mathbf{z}(l)$ and $\mathbf{z}(l)$ is the sample vector of the lth signal segment. The conjugate covariance function is given by

$$\hat{\mathbf{C}}^* = \frac{1}{L}\sum_{l=0}^{L-1}\mathbf{z}(l)\mathbf{z}^T(l) - \bar{\mathbf{z}}\bar{\mathbf{z}}^T. \tag{23}$$

Consequently, the CAF and the SCD estimate are obtained by [10]

$$\hat{R}_x(\alpha,\tau) = \left\{\frac{1}{N}\sum_{n=0}^{N-1-\tau}\hat{C}_x(n,\tau)e^{-j2\pi\alpha n/N}\right\}e^{-j\pi\alpha\tau/N}, \tag{24}$$

$$\hat{S}_x(\alpha,\mu) = \sum_{\tau=0}^{N-1}\hat{R}_x(\alpha,\tau)e^{-j2\pi\mu\tau/N}, \tag{25}$$

where n is the sample index, τ is the sample delay index, α and μ are respectively the digital cyclic frequency and the digital frequency, and $n, \tau, \alpha, \mu \in [0, N-1]$. The covariance value $\hat{C}_x(n,\tau)$ is taken from the element located at the $(n+1)$th row and the $(n+\tau+1)$th column of $\hat{\mathbf{C}}$. In the case of nonconjugate cyclostationarity as shown in Figs. 4 and 5, only the GMSK signal manifests itself. The cyclic features of the UWB signal are too weak to be observed. However, the cyclic features of the UWB signal are quite obvious for the conjugate cyclostationary case in Figs. 6 and 7. Due to the large bandwidth of the UWB signal, there are quite a number of cyclic frequencies as multiples of $1/T_s$. As the UWB pulse is narrow, the range of τ for the nonzero support of the CAF is small (less than 6 ns) in Fig. 6. Moreover, the frequency range for the nonzero support of the SCD is large because of the bandwidth as shown in Fig. 7, and the GMSK signal can be roughly observed as the double crosses embedded in the cyclic spectrum of the signal $z(t)$.

Assuming the knowledge of T_s, the UWB signal can be detected at the cycle set $\mathcal{A} = \{\alpha_q, q = 1, 2, \ldots M\}$, where $\alpha_q = q/T_s$, $M = \lfloor 2BT_s \rfloor$ and B is the bandwidth of the UWB signal. Since the GMSK signal is hardly observed in the conjugate CAF, we can accomplish the detection in time-domain using the estimated conjugate CAF $\hat{R}_x^*(\alpha_q, \tau)$. For certain τ, we check the cycle set. Thus, it is a multi-cycle detector. Let us define $\hat{\mathbf{r}} = [\hat{R}_x^*(\alpha_1,\tau), \ldots, \hat{R}_x^*(\alpha_M,\tau)]^T$. The hypotheses-testing problem is given by

$$\mathcal{H}_0 \quad : \quad \hat{\mathbf{r}} = \mathbf{e}, \tag{26}$$

$$\mathcal{H}_1 \quad : \quad \hat{\mathbf{r}} = \mathbf{r} + \mathbf{e}, \tag{27}$$

where $\mathbf{r}$ is the true nonrandom cyclic autocorrelation and $\mathbf{e}$ is the estimation error vector, which is asymptotically Gaussian distributed.

Therefore, the test statistic is then given by

$$T = M\hat{\mathbf{r}}^H\hat{\mathbf{\Sigma}}^{-1}\hat{\mathbf{r}}, \tag{28}$$

where $\hat{\mathbf{\Sigma}}$ is the estimated error covariance matrix following the method in [10]. Hence, under $\mathcal{H}_0$, the distribution of T asymptotically converges to the central χ^2 distribution with $2M$ degrees of freedom. Therefore, a threshold can be decided by the constant false alarm rate as $P_f = \mathrm{Prob}(T \geq \gamma)$.

Example 3: the performance of the detector is evaluated by simulations. The UWB pulse and the GMSK signal are the same as in the previous example. The symbol period of the UWB signal is 16 ns, then the basic cyclic frequency is 62.5 MHz. The segment length is 32 ns including two UWB symbols. Other parameters are the same as in the previous example. Fig. 8 illustrates the probability of detection vs. SIR with different false alarm ratios. Higher the false alarm ratio, higher the probability of detection. According to Fig. 8, the UWB signal can be detected even with very low SIR. Taking the benefit of the conjugate cyclostationary properties, the UWB signal can be distinguished from the GMSK signal.

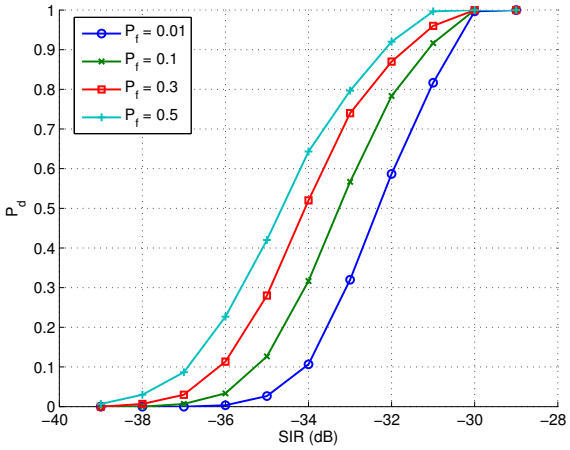

Fig. 8. Probability of detection P_d vs. SIR, with different false alarm ratios

V. Conclusions

In this paper, a multi-cycle detector based on conjugate cyclostationarity is proposed to detect a UWB signal under the existence of a GMSK signal. We first explore the cyclic feature of a generalized UWB IR signal, and show several examples of the cyclic spectrum of the BPPM UWB IRs with short DS and TH codes. By exploiting the nonconjugate and the conjugate cyclostationarity of the coexistence signals, we observe the dominance of the UWB signal in the conjugate cyclostationarity. As a result, a multi-cycle detector in time-domain making use of the conjugate cyclic autocorrelation is proposed to detect the UWB signal coexisted with the GMSK signal. The simulation results indicate the feasibility to detect the UWB signal that is overwhelmed by the GMSK signal.

Acknowledgment

Part of the work was supported by the Georgia Tech Ultra-wideband Center of Excellence (http://www.uwbtech.gatech.edu/).

References

[1] M. Hamalainen, V. Hovinen, R. Tesi, J.H.J. Iinatti, and M. Latva-aho, "On the UWB system coexistence with GSM900, UMTS/WCDMA, and GPS," *IEEE J. Sel. Areas Commun.*, vol. 20, no. 9, pp. 1712–1721, Dec. 2002.

[2] S.M. Mishra, R.W. Brodersen, S.T. Brink, and R. Mahadevappa, "Detect and avoid: an ultra-wideband/WiMAX coexistence mechanism," *IEEE Commun. Mag.*, vol. 45, no. 6, pp. 68–75, June 2007.

[3] A. Tani and R. Fantacci, "A low-complexity cyclostationary-based spectrum sensing for UWB and WiMAX coexistence with noise uncertainty," *IEEE Trans. Veh. Technol.*, vol. 59, no. 6, pp. 2940–2950, July 2010.

[4] W. A. Gardner, "Exploitation of spectral redundancy in cyclostationary signals," *IEEE Signal Process. Mag.*, vol. 8, no. 2, pp. 14–36, Apr. 1991.

[5] A. V. Dandawate and G. B Giannakis, "Statistical tests for presence of cyclostationarity," *IEEE Trans. Signal Process.*, vol. 42, no. 9, pp. 2355–2369, Sept. 1994.

[6] G. B. Giannakis, *Cyclostationary signal analysis*, Boca Raton, FL: CRC, 1998.

[7] J. Lundén, V. Koivunen, A. Huttunen, and H.V. Poor, "Collaborative cyclostationary spectrum sensing for cognitive radio systems," *IEEE Trans. Signal Process.*, vol. 57, no. 11, pp. 4182–4195, Nov. 2009.

[8] Sung Hwan Sohn, Ning Han, Jae Moung Kim, and Jae Wan Kim, "Ofdm signal sensing method based on cyclostationary detection," in *Proc. CrownCom*, 2007, pp. 63–68.

[9] M. Oner and F. Jondral, "On the extraction of the channel allocation information in spectrum pooling systems," *IEEE J. Sel. Areas Commun.*, vol. 25, no. 3, pp. 558–565, Apr. 2007.

[10] Z. Tian, Y. Tafesse, and B. M. Sadler, "Cyclic feature detection with sub-Nyquist sampling for wideband spectrum sensing," *IEEE J. Sel. Topics in Signal Processing*, vol. 6, no. 1, pp. 58–69, Feb. 2012.

[11] M. Oner, "On the spectral correlation of UWB impulse radio signals," *IEEE Commun. Lett.*, vol. 12, no. 10, pp. 714–716, Oct. 2008.